EPJ A
Hadrons and Nuclei

EPJ.org
your physics journal

Eur. Phys. J. A (2017) **53**: 37 DOI 10.1140/epja/i2017-12228-3

Relativistic diffusion model with nonlinear drift

F. Forndran and G. Wolschin

Società Italiana di Fisica

Springer

Eur. Phys. J. A (2017) **53**: 37
DOI 10.1140/epja/i2017-12228-3

THE EUROPEAN PHYSICAL JOURNAL A

Regular Article – Theoretical Physics

Relativistic diffusion model with nonlinear drift

F. Forndran and G. Wolschin[a]

Institut für Theoretische Physik der Universität Heidelberg, Philosophenweg 16, D-69120 Heidelberg, Germany

Received: 3 November 2016 / Revised: 7 February 2017
Published online: 27 February 2017 –
Communicated by G. Torrieri

Abstract. The nonequilibrium-statistical Relativistic Diffusion Model (RDM) is extended to include a nonlinear drift term such that its stationary solution agrees exactly with the thermal equilibrium distribution. The underlying Fokker-Planck equation cannot be solved analytically in this case and we present a numerical solution in rapidity space. The difference to the analytical RDM solution is discussed, and the numerical result is compared to data for net-proton rapidity distributions in $\sqrt{s_{NN}} = 17.3$ GeV PbPb and 200 GeV AuAu collisions.

The relativistic diffusion model (RDM) provides a phenomenological nonequilibrium-statistical description of distribution functions for produced particles as well as for net baryons and net protons (protons minus produced antiprotons) in relativistic heavy-ion collisions. Inspite of its simplicity and analytical solvability, the model has predictive properties in particular for rapidity distributions at higher LHC energies such as 5.02 TeV PbPb at the Large Hadron Collider (LHC).

The RDM in its original form makes use of a generalized diffusion equation of the Fokker-Planck type as introduced by Smoluchowski [1]. Similar to the Uhlenbeck-Ornstein process [2], it is based on a linear ansatz for the drift term with a relaxation time τ_y in rapidity space, or a corresponding friction coefficient [3–6]. To describe stopping in a relativistic heavy-ion collision, two fragmentation sources occur for net baryons, or for net protons, that both experience diffusion processes in rapidity space caused by scatterings and particle creations. The fragmentation distributions are microscopically due to valence quark-gluon interactions [7].

In case of produced charged hadrons, an additional midrapidity source appears which is mainly due to gluon-gluon interactions, with a total particle content that depends on the cube of the logarithmic center-of-mass energy [5]. It is affected by the drift term as well, although its mean value drifts only in case of asymmetric systems as has been investigated in [8,9]. Symmetric systems had also been considered in [10] and subsequent works. The model accounts for the broad and —for produced particles— often flat rapidity distributions, whereas other macroscopic models such as the thermal model fail to do that.

The RDM is in scope located between equilibrium-statistical models for multiple hadron production as originally proposed by Hagedorn [11], and more detailed numerical models such as hydrodynamics (*e.g.*, [12–16]). Depending upon the description of the initial state in viscous hydrodynamic approaches, the calculated rapidity spectra of produced charged hadrons may turn out to be too narrow [17], indicating the fact that a three-source approach is needed that also accounts for target- and projectile-like fluids. Indeed such models have been developed (*e.g.*, [18–20]) and provide reasonable descriptions for produced-particle spectra and also for stopping (baryon minus antibaryon, or proton minus antiproton) distribution functions. A related three-source approach is the basis of the relativistic diffusion model.

Although the stationary solution of the RDM at high temperature T is very close to the required Boltzmann distribution, it does not exactly match it. This fact is a consequence of the linear ansatz for the drift term. In this work we therefore develop a numerical solution of a Fokker-Planck equation (FPE) with a nonlinear drift term and a corresponding stationary solution that equals the Boltzmann distribution, investigate its consequences, and compare with net-proton rapidity distributions from central PbPb collisions at $\sqrt{s_{NN}} = 17.3$ GeV and central AuAu collisions at $\sqrt{s_{NN}} = 200$ GeV. Here we focus in particular on the nonequilibrium-statistical aspects, whereas the presence of collective effects (flow) is accounted for by phenomenological values of the diffusion coefficients when comparing to data.

1 Theoretical model

In relativistic heavy-ion physics the additive variable rapidity replaces the velocity. It is defined by

$$y = \frac{1}{2} \ln \left(\frac{E + p_\parallel}{E - p_\parallel} \right), \tag{1}$$

[a] e-mail: wolschin@uni-hd.de

where E is the laboratory energy and $p_\parallel$ the momentum along the beam axis —in this case the z-axis. With the relativistic energy-momentum relation ($E^2 = p^2 + m^2$) we can express E and $p_\parallel$ in terms of y:

$$E = m_\perp \cosh(y), \tag{2}$$
$$p_\parallel = m_\perp \sinh(y), \tag{3}$$

where $m_\perp = \sqrt{m^2 + p_\perp^2}$ is the transverse mass and $p_\perp = \sqrt{p_x^2 + p_y^2}$ the transverse momentum. For the purpose of this work the invariant differential cross-section or invariant yield is the key variable, since it is invariant under Lorentz boosts. It is given by (using eq. (2) and eq. (3))

$$\begin{aligned}\frac{\mathrm{d}^3N}{\mathrm{d}p^3} &= \frac{\mathrm{d}^3N}{\mathrm{d}p_x\mathrm{d}p_y\mathrm{d}p_z} \\ &= \frac{\mathrm{d}^3N}{p_\perp \mathrm{d}p_\perp \mathrm{d}\phi \mathrm{d}p_\parallel} = \frac{\mathrm{d}^2N}{2\pi p_\perp \mathrm{d}p_\perp \mathrm{d}(m_\perp \sinh(y))} \\ &= \frac{\mathrm{d}^2N}{2\pi p_\perp \mathrm{d}p_\perp m_\perp \cosh(y)\mathrm{d}y} = \frac{\mathrm{d}^2N}{2\pi p_\perp \mathrm{d}p_\perp E \mathrm{d}y}\end{aligned}$$

and hence

$$E\frac{\mathrm{d}^3N}{\mathrm{d}p^3} = \frac{\mathrm{d}^2N}{2\pi p_\perp \mathrm{d}p_\perp \mathrm{d}y} = \frac{\mathrm{d}^2N}{2\pi m_\perp \mathrm{d}m_\perp \mathrm{d}y}\,. \tag{4}$$

Therefore the rapidity distribution is obtained as

$$\frac{\mathrm{d}N}{\mathrm{d}y}(y,t) = C\int m_\perp E\frac{\mathrm{d}^3N}{\mathrm{d}p^3}\mathrm{d}m_\perp, \tag{5}$$

with a normalisation constant C.

The global thermodynamical concept is given by the Boltzmann approximation for a single particle distribution since the system's freeze-out temperature exceeds 100 MeV. Considering eq. (2) the thermal Boltzmann distribution can be rewritten in terms of rapidity y and transverse mass $m_\perp$

$$E\frac{\mathrm{d}^3N}{\mathrm{d}p^3} \propto Ee^{-E/T} = m_\perp \cosh(y) e^{-m_\perp \cosh(y)/T}, \tag{6}$$

where T is the temperature. On the other hand, with eq. (5) the thermal equilibrium distribution for the rapidity follows as

$$\begin{aligned}\frac{\mathrm{d}N_\mathrm{eq}}{\mathrm{d}y} = C\left[m_\perp^2 T + \frac{2m_\perp T^2}{\cosh(y)} + \frac{2T^3}{\cosh^2(y)}\right] \\ \times \exp\left(-\frac{m_\perp \cosh(y)}{T}\right).\end{aligned} \tag{7}$$

The stationary solution of the transport equation that accounts for the approach towards thermal equilibrium should agree with the isotropic thermal equilibrium solution eq. (7), where T is identified with the system's freeze-out temperature. For a rapidity distribution $f(y,t)$ we write the nonequilibrium-statistical Fokker-Planck equation as

$$\frac{\partial f(y,t)}{\partial t} = -\frac{\partial}{\partial y}\left[J(y)f(y,t)\right] + D\frac{\partial^2}{\partial y^2}f(y,t) \tag{8}$$
$$= -\frac{\partial}{\partial y}\left\{J(y)f(y,t) - D\frac{\partial}{\partial y}f(y,t)\right\}, \tag{9}$$

with a time-independent drift term $J(y)$ and a constant diffusion coefficient D. In eq. (9) the FPE is recast as a conservation law, with a density $f(y,t)$ and a flux $w(y,t) = J(y)f(y,t) - D\frac{\partial}{\partial y}f(y,t)$.

For the relativistic diffusion model [3] a relaxation ansatz for the drift had been made

$$J(y) = \frac{y_\mathrm{eq} - y}{\tau_y} \tag{10}$$

with the equilibrium rapidity y_eq and a relaxation time τ_y. The resulting FPE is, with $R(y,t)$ replacing $f(y,t)$

$$\frac{\partial}{\partial t}R(y,t) = \frac{\partial}{\partial y}\left[\frac{y - y_\mathrm{eq}}{\tau_y}R(y,t)\right] + D\frac{\partial^2}{\partial y^2}R(y,t). \tag{11}$$

Equation (11) has an exact analytical solution. The Fourier transform of eq. (11) is

$$\frac{\partial}{\partial t}\tilde{R}(k,t) + \frac{k}{\tau_y}\frac{\partial}{\partial k}\tilde{R}(k,t) = \left[\frac{ik}{\tau_y}y_\mathrm{eq} - k^2D\right]\tilde{R}(k,t), \tag{12}$$

where $\tilde{R}(k,t)$ is the Fourier transform of $R(y,t)$. This is a partial differential equation of first order in k and t and therefore solvable with the method of characteristics. This results in

$$\frac{\mathrm{d}}{\mathrm{d}t}\tilde{R}(k_0,t) = \left[\frac{ik_0e^{t/\tau_y}}{\tau_y} - Dk_0^2e^{2t/\tau_y}\right]\tilde{R}(k_0,t), \tag{13}$$

with $k_0 = ke^{-t/\tau_y}$. After separation of the unknowns the solution of eq. (12) is

$$\begin{aligned}\tilde{R}(k_0,t) = \tilde{R}(k_0,0)\exp\Bigg[ik_0y_\mathrm{eq}(e^{t/\tau_y} - 1) \\ -\frac{D\tau_y}{2}k_0^2(e^{2t/\tau_y} - 1)\Bigg].\end{aligned} \tag{14}$$

The widths of the initial peaks are determined by the Fermi velocity v_F, since the fermions in the incident nuclei have a non-zero velocity and therefore a non-zero width in rapidity space: for a Fermi energy of 38 MeV the corresponding Fermi velocity is $v_\mathrm{F} = 0.28$, with an ensuing width (FWHM) in rapidity space of $\Gamma = \tanh^{-1}(0.28) \simeq 0.281$. Hence Gaussian distributions with a finite standard deviation $\sigma = \Gamma/\sqrt{8\ln 2}$ are considered as initial condition. They are given by

$$R(y,0) = \frac{1}{\sqrt{2\pi\sigma^2}}\exp\left[-\frac{(y - y_0)^2}{2\sigma^2}\right] \tag{15}$$

with the mean y_0, representing the beam rapidity.

The initial function in Fourier space $\tilde{R}(k_0, 0)$ is obtained with a Fourier transform of eq. (15)

$$\tilde{R}(k_0, 0) = \frac{1}{\sqrt{2\pi}} \exp\left[-\frac{\sigma^2 k^2}{2} - iky_0\right]. \quad (16)$$

Without loss of generality, only the initial condition with mean at $y = +y_0$ is used in the following and for eq. (14). After an inverse Fourier transformation of eq. (14) the exact solution of eq. (11) is obtained

$$R(y, t) = \frac{1}{\sqrt{2\pi\sigma_y^2}} \exp\left[-\frac{(y - \langle y\rangle)^2}{2\sigma_y^2}\right] \quad (17)$$

with mean value

$$\langle y\rangle = y_0 e^{-t/\tau_y} + y_{\rm eq}(1 - e^{-t/\tau_y}) \quad (18)$$

and variance

$$\sigma_y^2 = \sigma^2 e^{-2t/\tau_y} + D\tau_y(1 - e^{-2t/\tau_y}). \quad (19)$$

This model is successfully used to describe rapidity spectra of heavy-ion collisions by multiplying each source with the corresponding number of charged particles. For the rapidity spectra of produced particles $\frac{{\rm d}N}{{\rm d}y}$ it is essential to consider a three-sources model with the two fragmentation sources $\delta(y \mp y_0)$ and a midrapidity source at $y_{\rm eq}$. All three sources correspond to an own solution of eq. (11), which can be added incoherently due to the linearity of the PDE. However, the RDM is also used to describe net-proton or net-baryon rapidity distributions, where the midrapidity source is absent.

For simplification the initial Gaussian distribution is often approximated as a δ-peak at y_0. Then the solution becomes

$$R(y, t) = \frac{1}{\sqrt{2\pi\bar{\sigma}^2}} \exp\left[-\frac{(y - \bar{y})}{2\bar{\sigma}^2}\right], \quad (20)$$

with

$$\bar{y} = y_0 e^{-t/\tau_y} + y_{\rm eq}(1 - e^{-t/\tau_y}), \quad (21)$$

$$\bar{\sigma}^2 = D\tau_y(1 - e^{-2t/\tau_y}). \quad (22)$$

These results differs from the previous ones only in the standard deviations (σ and $\bar{\sigma}$) and for larger times the two solution functions are nearly identical. In the following, the distribution with the initial Gaussian will be used, since it is physically more appropriate.

2 Stationary solution of the RDM

The stationary solution of eq. (11) for $t \to \infty$ obeys the following differential equation:

$$\frac{1}{D\tau_y}\frac{\partial}{\partial y}\left[(y_{\rm eq} - y)R_{\rm st}(y)\right] = \frac{\partial^2}{\partial y^2}R_{\rm st}(y), \quad (23)$$

solved by

$$R_{\rm st}(y) = \frac{1}{\sqrt{2\pi D\tau_y}} \exp\left[-\frac{1}{2D\tau_y}(y - y_{\rm eq})^2\right]. \quad (24)$$

This stationary solution differs from the thermal equilibrium Boltzmann distribution, introduced in eq. (7), although the difference is small. The nonlinear drift term that is required for the stationary solution to agree with the thermal equilibrium distribution can be obtained from the general linear FPE, eq. (8), with the stationary solution function $f_{\rm st}(y, t)$

$$\frac{\partial}{\partial y}\left[J(y)f_{\rm st}(y)\right] = D\frac{\partial^2}{\partial y^2}f_{\rm st}(y). \quad (25)$$

The drift is straightforwardly determined as [21]

$$J(y) = -\frac{m_\perp D}{T}\sinh(y), \quad (26)$$

with $f_{\rm st}(y) = \exp(-\frac{m_\perp \cosh(y)}{T})$, where the Einstein relation $D = bT$ (b the mobility of the particle) is used. This leads to a modified FPE

$$\frac{\partial}{\partial t}f(y, t) = \frac{m_\perp D}{T}\frac{\partial}{\partial y}\left[\sinh(y)f(y, t)\right] + D\frac{\partial^2}{\partial y^2}f(y, t), \quad (27)$$

with the solution function $f(y, t)$. Writing the amplitude of the drift term as

$$A = m_\perp D/T \quad (28)$$

the dissipation-fluctuation theorem with the mobility $b = A/m_\perp$ becomes

$$D = AT/m_\perp. \quad (29)$$

According to eq. (5) the corresponding rapidity spectrum is determined through

$$\frac{{\rm d}N}{{\rm d}y}(y, t) = C\int_m^\infty m_\perp^2 \cosh(y)f(y, t)\,{\rm d}m_\perp. \quad (30)$$

With the nonlinear drift the problem cannot be solved analytically anymore. The numerical solution for Dirichlet boundary conditions with values zero and initial Gaussian distributions to account for the Fermi motion is discussed in the next section.

3 Numerical solution

For the solution of eq. (27) the modular toolbox DUNE is chosen (Distributed and Unified Numerics Environment, `https://www.dune-project.org/`), which is a C++ framework for solving partial differential equations (PDE) using grid based methods, [22] and references therein. The numerical solution uses the finite element method. All implementations run on a one-dimensional grid with sizes adjusted to the problem.

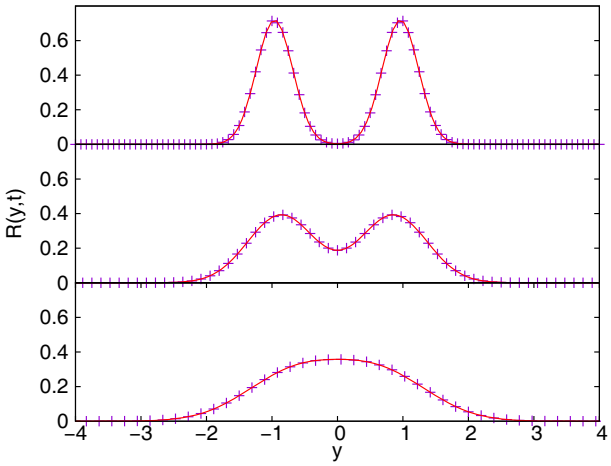

Fig. 1. (Color online) Comparison of analytical solutions of the linear FPE based on a relaxation ansatz (solid lines) with the corresponding numerical solutions obtained in this work (crosses). In the upper frame for $t = 4\Delta t$, in the middle frame for $t = 15\Delta t$ and in the lower frame for $t = 40\Delta t$, with $\Delta t = 0.01\,\mathrm{s}$. For clarity not all points of the numerical solutions are shown.

As a test of the numerical implementation, we have first solved the FPE with a linear drift, eq. (11), and compared with the exact analytical result, fig. 1. The solutions are found to be identical. At short times the two separate peaks do not affect each other, with increasing time the mean values of the solution functions drift towards midrapidity, in this case $y = 0$, and overlap. This superposition leads to a single distribution at the end. In heavy-ion physics these two initial peaks are identified with two incoming particle beams, which collide and form new particles from the relativistic energy. Additional test with *e.g.* a diffusion equation without drift also confirm that the numerical implementation reproduces the exact analytical solutions.

Hence the DUNE framework can be applied for solving the FPE with nonlinear drift coefficient. Nevertheless it is necessary to choose the right parameters for the numerical approach since, *e.g.*, the so-called global refinement parameter [22] can yet have an effect on the outcome. In the numerical solution of the FPE with nonlinear drift (eq. (27)) the time evolution appears quite similar to the one of the linear FPE: two sharp peaks evolve with time, broaden, eventually overlap and finally form a single distribution.

There are, however, differences in the detailed time evolution. In particular, the nonlinear drift coefficient produces a somewhat more rapid approach towards statistical equilibrium since it is determined by the hyperbolic sine: The absolute value of the nonlinear drift is greater than the drift caused by the relaxation ansatz for every rapidity y. Also, the numerical solution for each source is not an exact Gaussian anymore.

The numerical stationary solution of the nonlinear FPE now agrees with the exponential part of the Boltzmann distribution eq. (6), $\exp(-E/T)$, as shown in fig. 2.

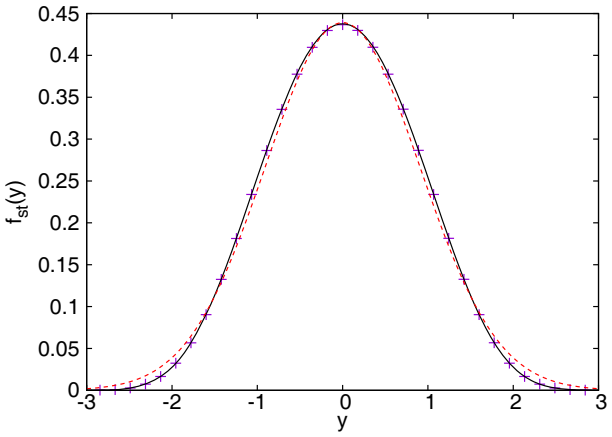

Fig. 2. (Color online) Stationary numerical solution of the FPE with nonlinear drift eq. (27) (crosses) compared to the exponential part of the Boltzmann distribution (solid line), and the stationary solution eq. (24) of the linear FPE (dashed line). Curves are normalized to the maximum value.

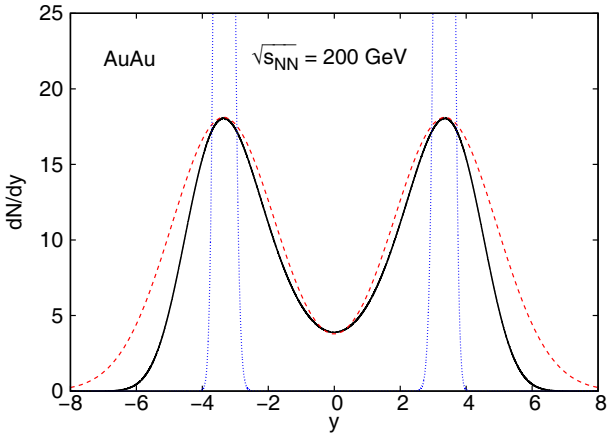

Fig. 3. (Color online) Rapidity distribution with nonlinear drift (solid curve) compared with the analytical solution of the linear RDM (dashed curve). The numerical distribution is shown for $t_{int} = 1.45 \times 10^{-23}\,\mathrm{s}$, $D = 30 \times 10^{23}\,\mathrm{s}^{-1}$ and the size of the drift scaled with a factor of 0.6, while the analytical distribution is shown for $t_{int}/\tau_y = 0.56$ and $D = 0.8 \times 10^{23}\,\mathrm{s}^{-1}$; the scaling of the drift equalizes the peak positions for this comparison. The dotted curves represent the numerical solutions using a theoretical diffusion coefficient as calculated from the dissipation-fluctuation theorem with the corresponding drift.

The difference to the stationary solution of the linear problem eq. (24), dashed curve, is seen to be rather small, it is most pronounced in the tails. However, when calculating rapidity distributions from eq. (30) the additional weighting factor $m_\perp^2 \cosh(y)$ augments the difference, see fig. 3 for the time-dependent case.

When applied to a relativistic heavy-ion collision, the value of the relaxation time in the linear model, or the amplitude of the drift term in the nonlinear model will be determined from the position of the stopping peaks in rapidity space. For identical peak positions and adjusted diffusion coefficients as shown in fig. 3, the distribution functions are then found to be somewhat different, with

the Gaussian analytical solution of the linear model having a slightly larger width than the non-Gaussian numerical solution of the nonlinear case.

For a given drift, we can also compute the diffusion coefficient from the dissipation-fluctuation theorem eq. (29) to obtain a theoretical value D_{th} as shown in fig. 3, see the curves with small widths. In comparison with relativistic heavy-ion data, the widths calculated from D_{th} always turn out to be too small because they do not account for collective expansion [23]. It has been attempted [21] to accomodate the large widths through a nonlinearity of the diffusion term with an exponent $2-q$ ($q<1.5$), but this would imply using the so-called nonextensive statistics rather than Boltzmann statistics. In this work we determine the widths from the data, with corresponding diffusion coefficients D_{exp}.

4 Comparison with stopping data

The FPE with the nonlinear drift is now applied to describe relativistic heavy-ion data for the stopping phase. We consider as examples the results of the net-proton yield in PbPb collisions (0–5% centrality) at $\sqrt{s_{\rm NN}}=17.3\,\mathrm{GeV}$ from the NA49 Collaboration at the SPS, see [24] and in central AuAu collisions at $\sqrt{s_{\rm NN}}=200\,\mathrm{GeV}$ [25]. Since the implementation requires numerical values for all coefficients, it is necessary to set the parameters in the equation to physically reasonable values before running the program.

The parameters for the initial distribution are y_0 and the initial standard deviation σ. We determine y_0 from the beam rapidities

$$y_{\rm beam}=\mp y_0=\mp\ln\left(\frac{\sqrt{s_{\rm NN}}}{m_{\rm p}}\right) \tag{31}$$

with the center-of-mass energy per nucleon pair $\sqrt{s_{\rm NN}}$ and the mass of the proton $m_{\rm p}=0.938\,\mathrm{GeV}$. This yields $y_0=\mp2.915$ for PbPb and $y_0=\mp5.362$ for AuAu. The initial width Γ (FWHM) is obtained from the Fermi velocity $v_{\rm F}\simeq0.28$ as $\Gamma=\tanh^{-1}(v_{\rm F})\simeq0.281$.

For the temperature T a value of 160 MeV is assumed, since this is approximately the crossover temperature which determines the transition from hadronic matter to the quark-gluon plasma. For AuAu the transverse mass $m_\perp$ is obtained from the $p_\perp$-spectra given by the BRAHMS Collaboration. As proposed in [25], Gaussians are fitted to the invariant yields, thereby changing the $p_\perp$-spectra to $m_\perp$-spectra using $m_\perp=\sqrt{m_{\rm p}^2+p_\perp^2}$ and eq. (4) for the yields. The results for protons and antiprotons are averaged to obtain

$$\langle m_\perp\rangle=(1.15\pm0.20)\,\mathrm{GeV}. \tag{32}$$

In the following $\langle m_\perp\rangle$ is taken to be constant and the result is used for further calculations. The remaining parameter is the size of the drift term, which is determined by the peak position. The latter is taken to be $|y_{\rm peak}|=3.5$ for AuAu, and $|y_{\rm peak}|=1.3$ for PbPb as in [26]. The resulting values for the amplitude $A\equiv A_{\rm exp}$ of the drift term are given in table 1. For the interaction time an initial value is $t_{int}\sim1.67\cdot10^{-23}\,\mathrm{s}$ as in the linear RDM, although it is expected that the FPE with the nonlinear drift evolves faster over time.

Table 1. Parameters of the relativistic diffusion model with nonlinear drift for stopping in central collisions. The amplitude of the drift term $A\equiv A_{\rm exp}$ and the diffusion coefficient $D\equiv D_{\rm exp}$ are fitted to the data. The diffusion coefficients include collective expansion.

System	$\sqrt{s_{\rm NN}}$ (GeV)	$D_{\rm exp}$ ($10^{23}\,\mathrm{s}^{-1}$)	$A_{\rm exp}$ ($10^{23}\,\mathrm{s}^{-1}$)	$t_{\rm int}$ ($10^{-23}\,\mathrm{s}$)
PbPb	17.3	0.8	0.6	1.5
AuAu	200	30	3.62	1.45

As discussed previously, the theoretical diffusion coefficient $D\equiv D_{th}$ in a nonequilibrium-statistical model is determined from the drift coefficient and the temperature through the Einstein relations. It is well known, however, that this will underestimate [23] the actual width of the physical distributions since collective expansion leads to additional broadening beyond the purely thermal effect, see fig. 3.

Hence we determine the diffusion coefficient $D_{\rm exp}$ that is required from the data in an iterative procedure. An initial value is obtained from a fit of the linear relativistic diffusion model with respect to the data, resulting *e.g.* in a preliminary value $D\sim1\cdot10^{23}\,\mathrm{s}^{-1}$ for the diffusion constant in 200 GeV AuAu, and correspondingly for PbPb. The ensuing numerical solution $f(y,t)$ is then transformed into a rapidity spectrum by means of eq. (5)

$$\frac{\mathrm{d}N}{\mathrm{d}y}=C\int_m^\infty m_\perp^2\cosh(y)f(y,t)\,\mathrm{d}m_\perp, \tag{33}$$

where C is a normalisation constant determined by the number of participating protons $N_{\rm prot}$

$$C=\frac{N_{\rm prot}}{\int_{-\infty}^{\infty}\frac{\mathrm{d}N}{\mathrm{d}y}\,\mathrm{d}y}\,. \tag{34}$$

The mean number of participants is found from a Glauber calculation to be $N_{\rm part}=357\pm8$ [25] for the centrality class 0–5% in AuAu. Hence the number of protons is $N_{\rm prot}=\frac{79}{197}N_{\rm part}=143.2\pm3.2$ for central AuAu collisions at 200 GeV. Similarly, one obtains $N_{\rm prot}=141.4$ for central PbPb at 17.3 GeV. Next the value of the diffusion constant is adjusted iteratively until the widths of the experimental distributions are reproduced, with values given in table 1 and net-proton rapidity distribution functions shown in fig. 4. For both systems investigated here the experimental net-proton results are well represented, although there are discrepancies in the midrapidity region at higher energies such as for AuAu at 200 GeV which can only be resolved in a QCD-based approach as shown in [7].

When applying the relativistic diffusion model to produced particles rather than net-proton or net-baryon distributions, an additional central gluonic source appears

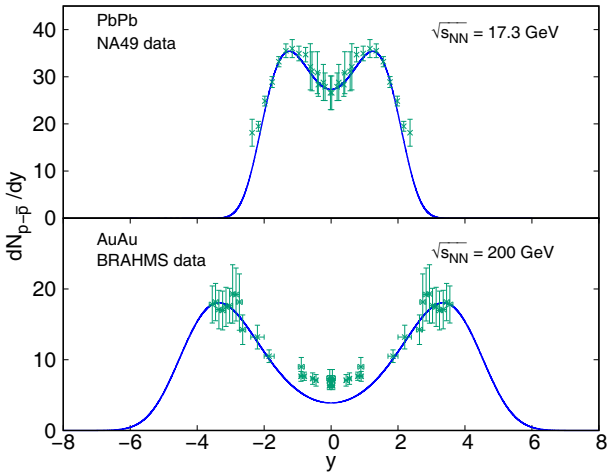

Fig. 4. (Color online) Numerical solution of the FPE with nonlinear drift for net-proton (proton minus antiproton) rapidity distributions. Upper frame: comparison with 17.3 GeV PbPb data from the NA49 Collaboration [24] at SPS. Lower frame: comparison with 200 GeV AuAu data from the BRAHMS Collaboration [25] at RHIC. The strength of the nonlinear drift term and the diffusion term are adjusted to the data, the values are given in table 1. The diffusion term includes additional broadening due to collective expansion. See text for the midrapidity region.

as discussed in the introduction. However, the behaviour of the rapidity distributions in their tails is still determined by the fragmentation sources, as is the case for net protons. In this region limiting fragmentation scaling [27] has been observed to hold for produced charged hadrons with considerable accuracy in pp and AA collisions [28–30] at RHIC energies: Particle production in the fragmentation region becomes essentially independent of the collision energy. The limiting fragmentation concept refers to particle production as function of rapidity y, but it also holds in pseudorapidity space since for $|\eta| \gg 1$ we have $y \simeq \ln(p_T/m_T) + \eta \simeq \eta$. (In the large-$\eta$ region, the Jacobian is very close to unity).

In [31] we had shown that the RDM with a linear drift does indeed fulfill limiting fragmentation in the tails of the centrality-dependent $\mathrm{d}N/\mathrm{d}\eta$-distributions for produced charged hadrons not only at RHIC, but also at LHC energies. This is in contrast to the thermal model that predicts a violation of extended longitudinal scaling at LHC energies [32], likely because in that model only an equilibrated fireball source is considered and the fragmentation sources that determine the tail behaviour are neglected. It should therefore be checked whether limiting fragmentation is also fulfilled in the nonlinear diffusion model for produced charged hadrons. In the case of net-proton stopping distributions that we discuss in this work, no data are available in the tail region above SPS energies so that a detailed comparison is not possible.

5 Conclusion and outlook

The relativistic diffusion model has been extended through a nonlinear drift term such that its stationary solution at high temperatures T agrees exactly with the Boltzmann distribution. We have solved the Fokker-Planck equation with nonlinear drift numerically by means of the DUNE framework. Various tests —in particular the comparison with the exact solution of the linear model— verify the accuracy of the numerical implementation.

The shapes of the experimental stopping distributions are reproduced by the numerical solutions where net-proton data are available, in particular, for PbPb collisions at $\sqrt{s_{NN}} = 17.3\,\mathrm{GeV}$ and AuAu at $\sqrt{s_{NN}} = 200\,\mathrm{GeV}$. Here the size of the drift is determined from the positions of the net-proton peaks in the stopping process. When the corresponding diffusion coefficients are calculated from the Einstein relations, the widths of the rapidity distributions are too small because the systems expands collectively. Hence we have determined the size of the diffusion coefficients from the available data.

This yields excellent results at c.m. energies below 200 GeV. At higher energies, discrepancies between the model and the data build up in the midrapidity region where the experimental yields turn out to be above the overlapping tails of the distribution functions. The resolution of these discrepancies is beyond a nonequilibrium-statistical approach, it requires a QCD-based framework.

Obviously comparisons with net-proton data in the TeV-region would be most welcome, but these seem to be out of reach due to the lack of a suitable forward spectrometer at the Large Hadron Collider. Instead measured pseudorapidity distribution functions $\mathrm{d}N_{ch}/\mathrm{d}\eta$ for produced charged hadrons —which do not require particle identification and are available at relatively small scattering angles, or large values of pseudorapidity— can be compared to the RDM-predictions.

In this case the emerging gluonic source for particle creation is the decisive midrapidity contribution and small inaccuracies from the fragmentation sources near midrapidity become less important. Indeed the RDM with its linear approximation of the drift term through the relaxation ansatz provides already reasonable predictions for $\mathrm{d}N_{ch}/\mathrm{d}\eta$-distributions of produced charged hadrons at 5.02 TeV PbPb collisions, although these results could be further refined using the nonlinear drift function discussed in this work.

This work has been partially supported by DFG through TRR 33.

References

1. M. Smoluchowski, Ann. Phys. **353**, 1103 (1916).
2. G.E. Uhlenbeck, L.S. Ornstein, Phys. Rev. **36**, 823 (1930).
3. G. Wolschin, Eur. Phys. J. A **5**, 85 (1999).
4. G. Wolschin, J. Phys. G **40**, 45104 (2013).
5. G. Wolschin, Phys. Rev. C **91**, 014905 (2015).
6. G. Wolschin, Phys. Rev. C **94**, 024911 (2016).
7. Y. Mehtar-Tani, G. Wolschin, Phys. Rev. Lett. **102**, 182301 (2009).
8. G. Wolschin, M. Biyajima, T. Mizoguchi *et al.*, Phys. Lett. B **633**, 38 (2006).
9. P. Schulz, G. Wolschin, Eur. Phys. J. A **51**, 18 (2015).

10. M. Biyajima, M. Ide, T. Mizoguchi *et al.*, Prog. Theor. Phys. **108**, 559 (2002).
11. R. Hagedorn, Nuovo Cimento Suppl. **3**, 147 (1965).
12. T. Koide, G.S. Denicol, P. Mota *et al.*, Phys. Rev. C **75**, 034909 (2007).
13. M. Luzum, P. Romatschke, Phys. Rev. C **78**, 034915 (2008).
14. B.H. Alver, C. Gombeaud, M. Luzum *et al.*, Phys. Rev. C **82**, 034913 (2010).
15. U. Heinz, R. Snellings, Annu. Rev. Nucl. Part. Sci. **63**, 123 (2013).
16. G. Denicol, A. Monnai, B. Schenke, Phys. Rev. Lett. **116**, 212301 (2016).
17. W. van der Schee, B. Schenke, Phys. Rev. C **92**, 064907 (2015).
18. A.A. Amsden, A.S. Goldhaber, F.H. Harlow *et al.*, Phys. Rev. C **17**, 2080 (1978).
19. R.B. Clare, D. Strottman, Phys. Rep. **141**, 177 (1986).
20. Y.B. Ivanov, V.N. Russkikh, V.D. Toneev, Phys. Rev. C **73**, 044904 (2006).
21. A. Lavagno, Physica A **305**, 238 (2002).
22. P. Bastian *et al.*, Kybernetika **46**, 294 (2010).
23. G. Wolschin, Europhys. Lett. **47**, 30 (1999).
24. NA49 Collaboration (C. Blume *et al.*), J. Phys. G **34**, 951 (2007).
25. BRAHMS Collaboration (I.G. Bearden *et al.*), Phys. Rev. Lett. **93**, 102301 (2004).
26. Y. Mehtar-Tani, G. Wolschin, EPL **94**, 62003 (2011).
27. J. Benecke, T. Chou, C. Yang *et al.*, Phys. Rev. **188**, 2159 (1969).
28. PHOBOS Collaboration (B.B. Back *et al.*), Phys. Rev. Lett. **91**, 052303 (2003).
29. PHOBOS Collaboration (B. Alver *et al.*), Phys. Rev. C **83**, 024913 (2011).
30. G. Torrieri, Phys. Rev. C **82**, 054906 (2010).
31. D.M. Röhrscheid, G. Wolschin, Phys. Rev. C **86**, 024902 (2012).
32. J. Cleymans, J. Strümpfer, L. Turko, Phys. Rev. C **78**, 017901 (2008).